ONLINE DATA SUPPLEMENT

Patterns of carbon-bound exogenous compounds in lung cancer patients and association with disease pathophysiology

Thomas Kunzke, Verena M. Prade, Achim Buck, Na Sun, Annette Feuchtinger, Marco Matzka, Isis E. Fernandez, Wim Wuyts, Maximilian Ackermann, Danny Jonigk, Michaela Aichler, Ralph A. Schmid, Oliver Eickelberg, Sabina Berezowska, Axel Walch

Contents:

Supplemental Table S1: Baseline characteristics for the squamous cell carcinoma (SQCC) cohort. (eval.=evaluation)

	Number of patients							
Factors	**Total cohort**	**metabo-lomics tumor**	**metabo-lomics stroma**	**survival available**	**PD-L1 eval.**	**CD3 eval.**	**CD8 eval.**	**γH2AX eval.**
Total	330	313	268	250	218	327	329	320
Gender								
Male	281 (85%)	266 (85%)	225 (84%)	211 (84%)	182 (83%)	279 (85%)	280 (85%)	272 (85%)
Female	49 (15%)	47 (15%)	43 (16%)	39 (16%)	36 (17%)	48 (15%)	49 (15%)	48 (15%)
Age, median (min–max)	69.0 (43.2-85.1)	69.2 (43.2-85.1)	69.0 (43.2-85.1)	68.2 (43.2-85.1)	68.9 (43.2-85.1)	69.1 (43.2-85.1)	69.0 (43.2-85.1)	69.3 (43.2-85.1)
pT stage								
T1a	27	25	25	18	22	27	27	25
T1b	45	43	36	36	25	45	45	42
T2a	106	104	87	83	66	106	106	103
T2b	51	49	40	39	35	50	51	50
T3	75	68	58	55	53	73	75	74
T4	26	24	22	19	17	26	25	26
pN stage								
N0	187	179	152	140	121	184	187	182
N1	105	99	84	83	72	105	104	101
N2	38	35	32	27	25	38	38	37

	Number of patients							
Factors	**Total cohort**	**metabo - lomics tumor**	**metabo-lomics stroma**	**survival available**	**PD-L1 eval.**	**CD3 eval.**	**CD8 eval.**	**γH2AX eval.**
M								
M0	321	304	262	243	211	318	320	312
M1	9	9	6	7	7	9	9	8
Stage								
IA	53 (16%)	52 (17%)	45 (17%)	36 (14%)	35 (16%)	53 (16%)	53 (16%)	50 (16%)
IB	68 (21%)	66 (21%)	56 (21%)	53 (21%)	41 (19%)	68 (21%)	68 (21%)	67 (21%)
IIA	70 (21%)	67 (21%)	59 (22%)	56 (22%)	47 (22%)	69 (21%)	70 (21%)	65 (20%)
IIB	49 (15%)	45 (14%)	34 (13%)	39 (16%)	33 (15%)	47 (14%)	49 (15%)	49 (15%)
IIIA	74 (22%)	68 (22%)	62 (23%)	54 (22%)	52 (24%)	74 (23%)	73 (22%)	74 (23%)
IIIB	7 (2%)	6 (2%)	6 (2%)	5 (2%)	3 (1%)	7 (2%)	7 (2%)	7 (2%)
IV	9 (3%)	9 (3%)	6 (2%)	7 (3%)	7 (3%)	9 (3%)	9 (3%)	8 (3%)
Grade								
G1	6	5	4	5	3	6	6	6
G2	163	156	129	125	108	162	162	161
G3	161	152	135	120	107	159	161	153

	Number of patients							
Factors	**Total cohort**	**metabo-lomics tumor**	**metabo-lomics stroma**	**survival available**	**PD-L1 eval.**	**CD3 eval.**	**CD8 eval.**	**γH2AX eval.**
Resection								
R0	287	273	234	214	189	284	287	279
R1	40	37	31	33	27	40	39	38
R2	3	3	3	3	2	3	3	3
Smoking								
Pack-years, median (min–max)	50 (2-200)	50 (2-200)	50 (5-200)	50 (2-200)	50 (2-200)	50 (2-200)	50 (2-200)	50 (2-200)
n.a.	91	85	83	52	59	91	91	85
current smoker	145	137	117	115	95	145	145	140
former smoker	128	122	99	107	82	125	127	125
never smoker	0	0	0	0	0	0	0	0
n.a.	57	54	52	28	41	57	57	55

Supplemental Table S2: Baseline characteristics for lung fibrosis fresh frozen tissues.

	Number of patients		
Factors	**Total cohort**	**lung tissue from healthy organ donors**	**IPF from explanted lungs**
Total	8	4	4
Gender			
Male	7	3	4
Female	1	1	0
Age, median (min–max)	52.0 (29.0-64.0)	45.0 (29.0 - 60.0)	53.0 (51.0 - 64.0)
Smoking			
Pack-years, median (min–max)	25 (10-36)	n.a.	25 (10-36)
n.a.	4	4	0
current smoker	n.a.	n.a.	n.a.
former smoker	n.a.	n.a.	n.a.
never smoker	n.a.	n.a.	n.a.
n.a.	8	4	4

Cohort was previously published by Sun *et al.* (doi: 10.1183/13993003.02314-2017)

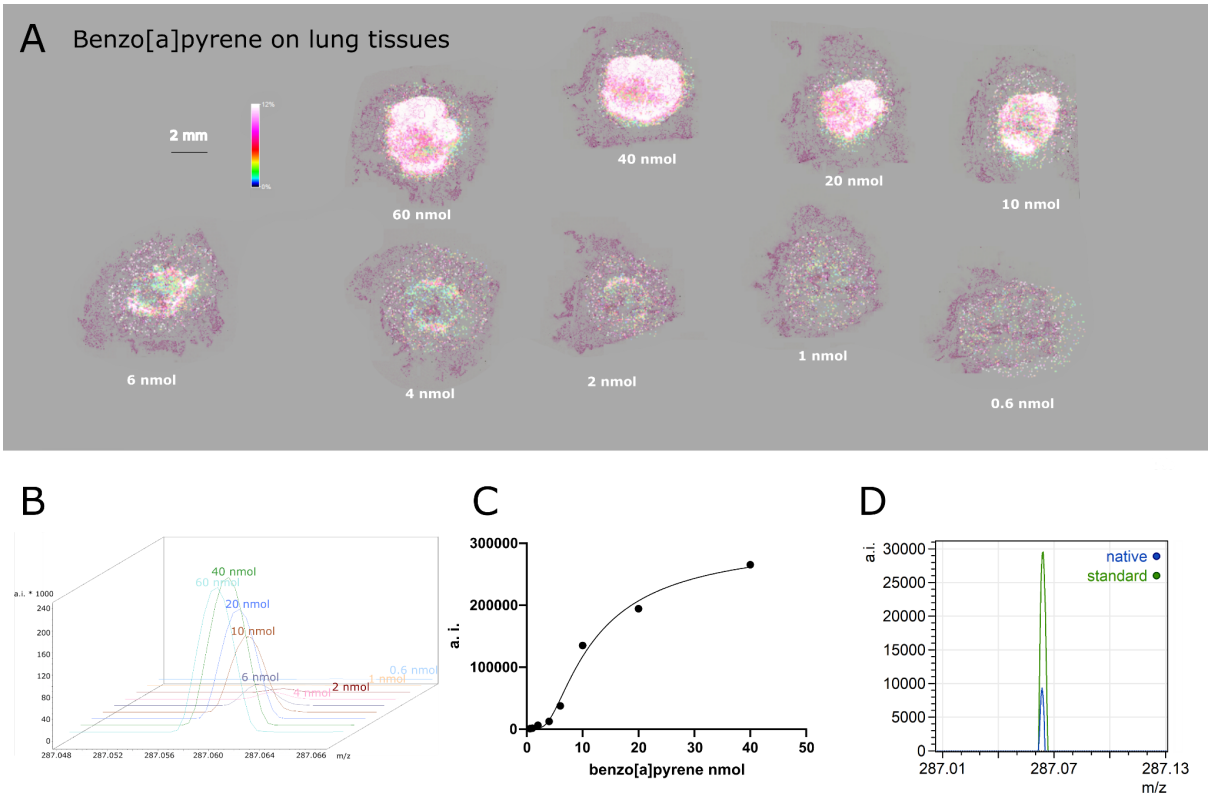

Supplemental Figure S1: On tissue measurement of benzo[a]pyrene. A: Benzo[a]pyrene was spotted onto human lung tissues. Labeled amount of substance refers to the absolute amount on lung tissue spotted by 1 µl benzo[a]pyrene solution. The minimum amount for detecting benzo[a]pyrene in human lung tissue samples is 2 nmol. **B:** Stack plot of the benzo[a]pyrene peak of different standard concentrations. **C:** Corresponding calibration curve of benzo[a]pyrene in human lung tissue samples. **D:** Measured native peak of benzo[a]pyrene in squamous-cell carcinoma tissues (*blue*) and comparison to standard benzo[a]pyrene peak (*green*).

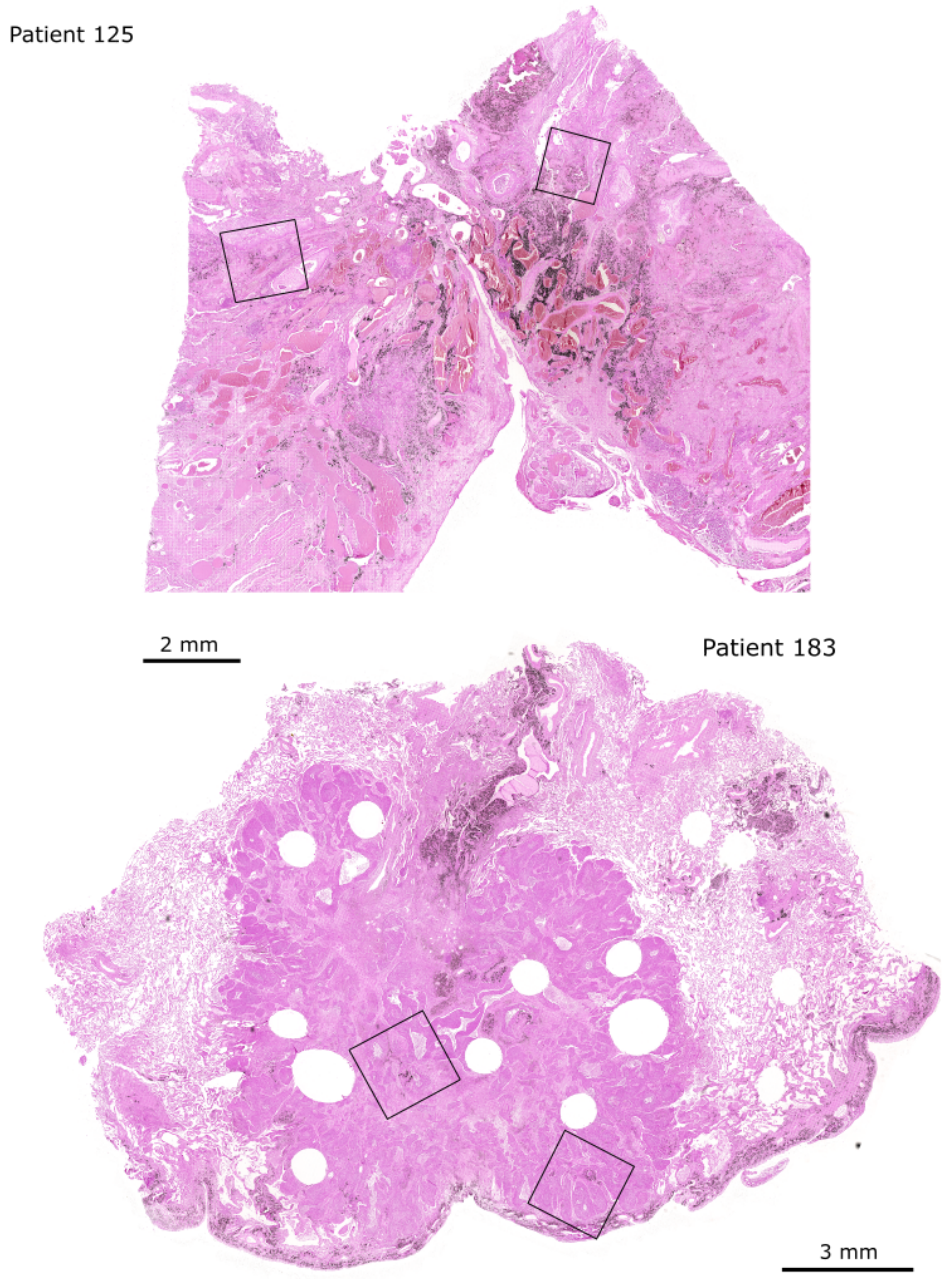

Supplemental Figure S2: Overview of whole-tissue section of patients 125 (top) and 183 (bottom). Tumor cell areas are highlighted and shown in Figure 3 at a higher magnification.

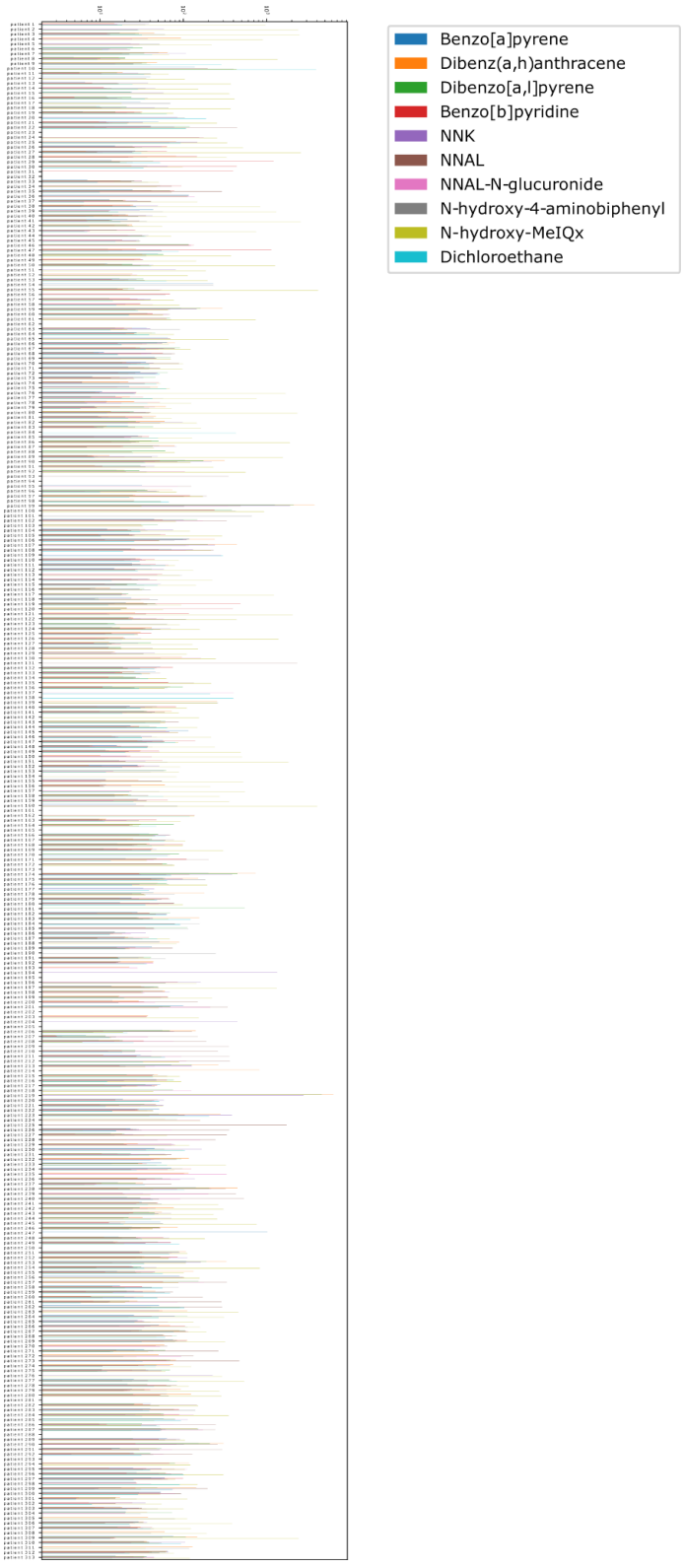

Supplemental Figure S3: Heterogeneity within exogenous compounds in tumor cell regions of all patients.

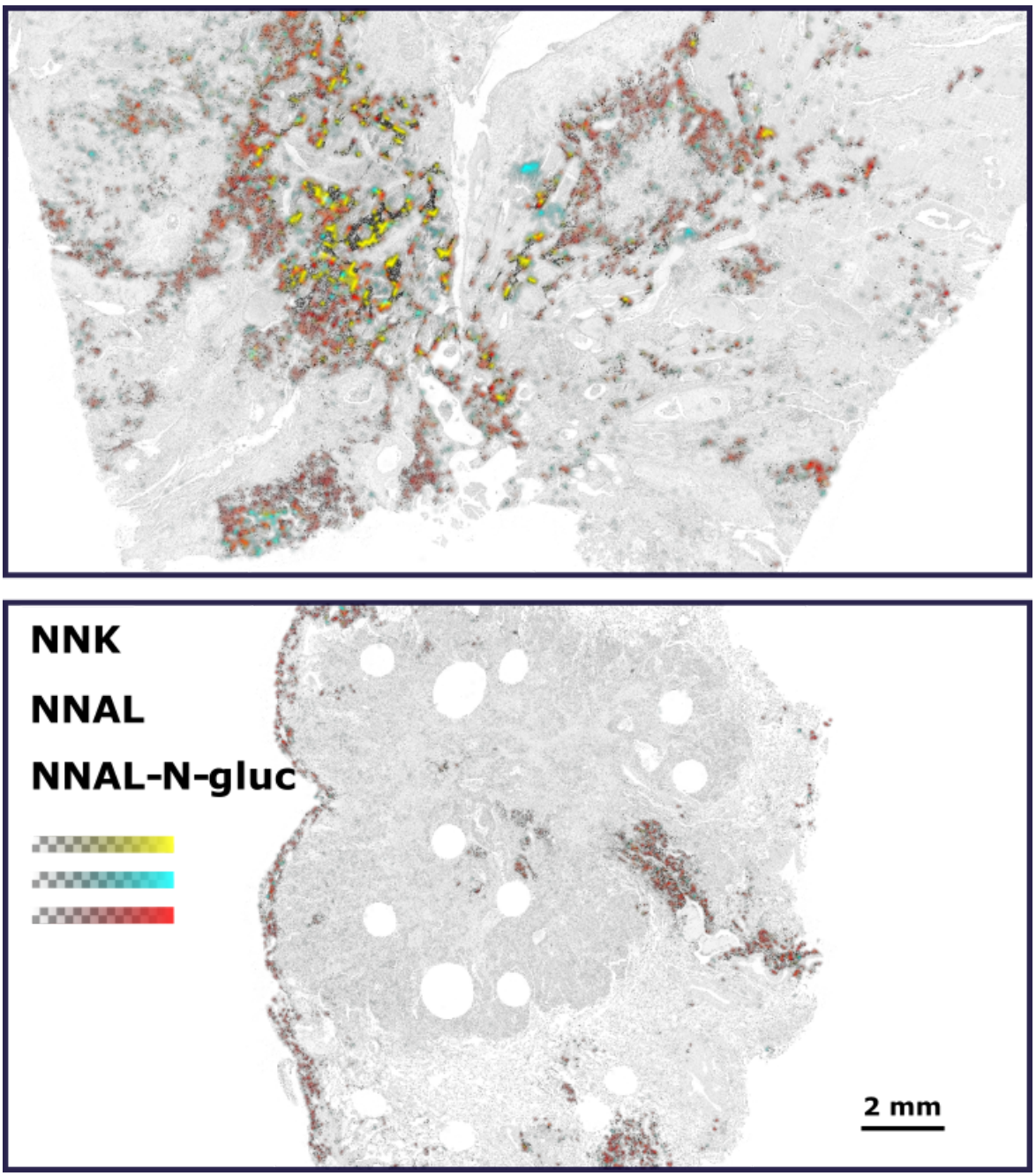

Supplemental Figure S4: Triple visualization of 4-(methylnitrosamino)-1-(3-pyridyl)-1-butanone (NNK), 4-methylnitrosamino)-1-(3-pyridyl)-1-butanol (NNAL), and NNAL-N-glucuronide demonstrates heterogeneity within two patient tissues. The same figure is shown in Figure 3 at a smaller magnification.

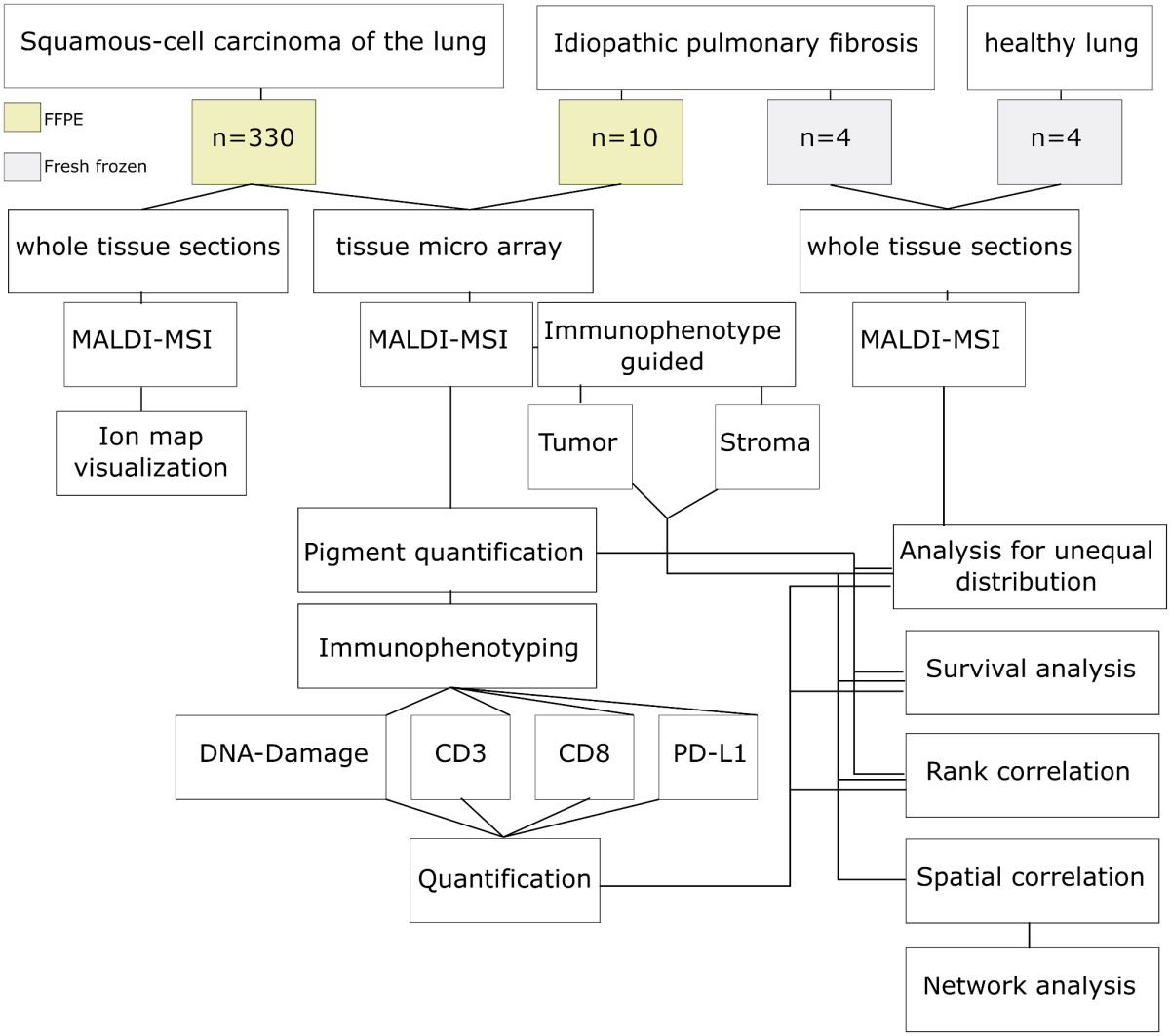

Supplemental Figure S5: Patient number, tissues and methods.

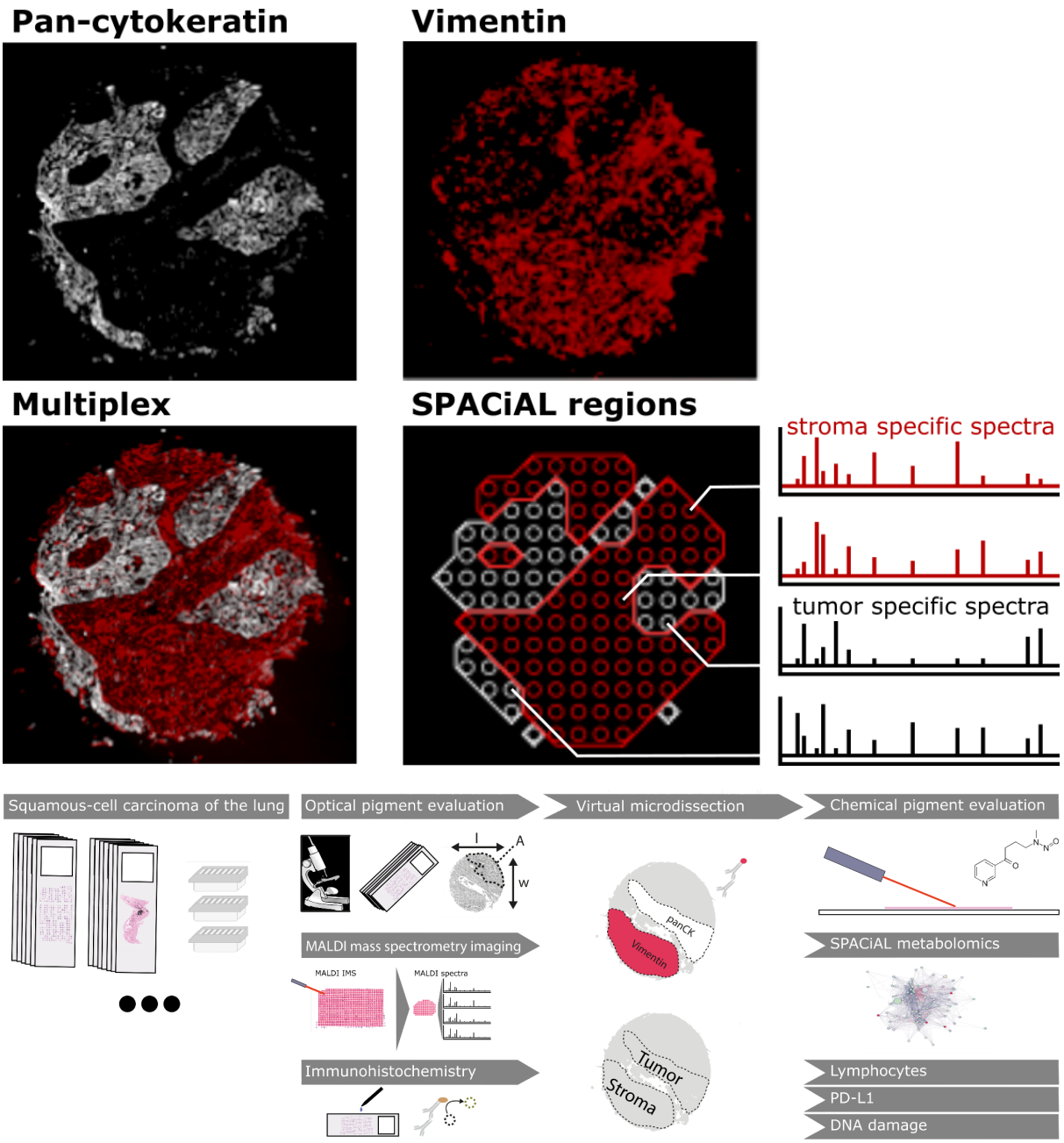

Supplemental Figure S6: Schematic procedure showing how spectra were automatically extracted from tumor or stroma regions in patients by immunophenotyping.

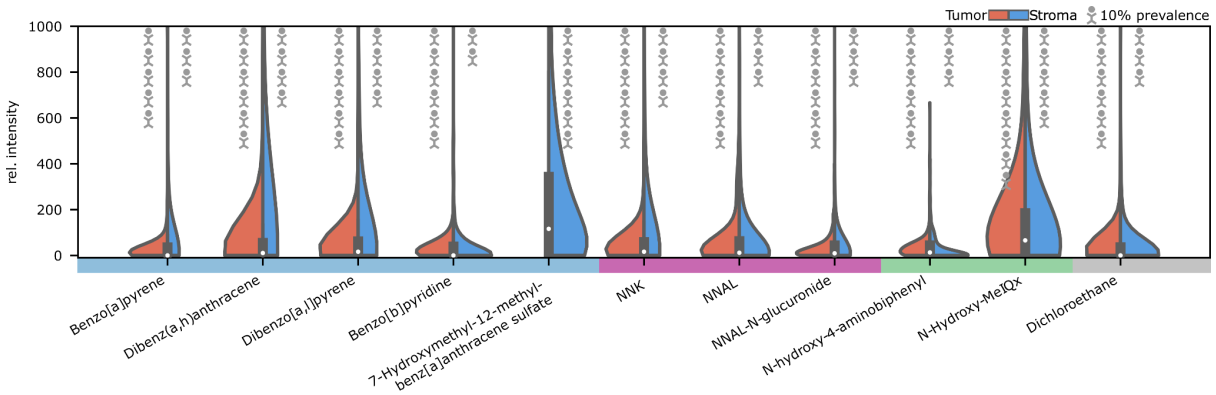

Supplemental Figure S7: Prevalence and distribution of carbon-bound compounds in the tumor (T) and stromal (S) regions.

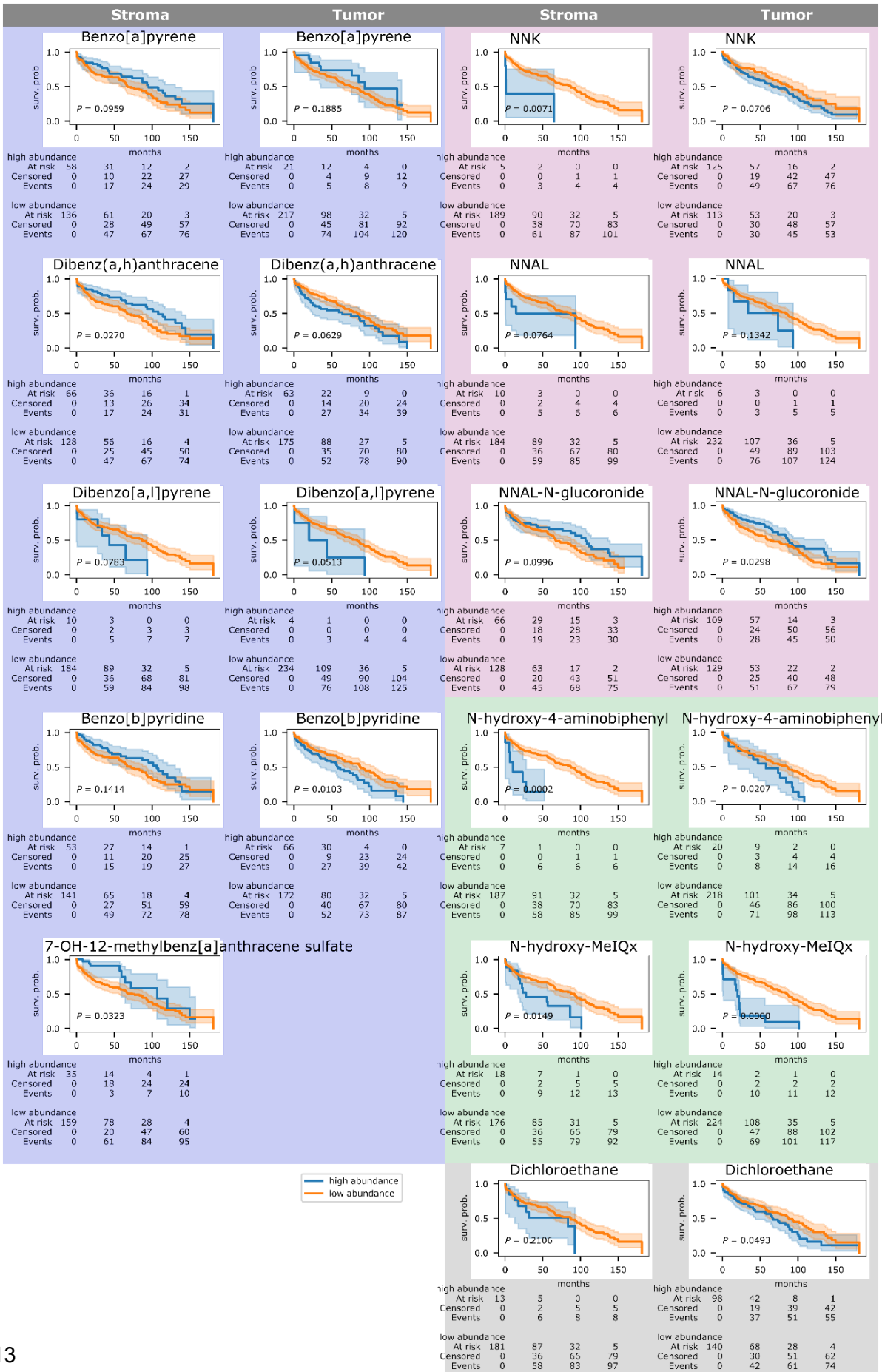
Stroma
Tumor
Stroma
Tumor
Benzo[a]pyrene
P = 0.0959
Benzo[a]pyrene
P = 0.1885
NNK
P = 0.0071
NNK
P = 0.0706
Dibenz(a,h)anthracene
P = 0.0270
Dibenz(a,h)anthracene
P = 0.0629
NNAL
P = 0.0764
NNAL
P = 0.1342
Dibenzo[a,l]pyrene
P = 0.0783
Dibenzo[a,l]pyrene
P = 0.0513
NNAL-N-glucoronide
P = 0.0996
NNAL-N-glucoronide
P = 0.0298
Benzo[b]pyridine
P = 0.1414
Benzo[b]pyridine
P = 0.0103
N-hydroxy-4-aminobiphenyl
P = 0.0002
N-hydroxy-4-aminobiphenyl
P = 0.0207
7-OH-12-methylbenz[a]anthracene sulfate
P = 0.0323
N-hydroxy-MeIQx
P = 0.0149
N-hydroxy-MeIQx
P = 0.0080
Dichloroethane
P = 0.2106
Dichloroethane
P = 0.0493
surv. prob.
months
high abundance
low abundance

Supplemental Figure S8: Kaplan–Meier survival analyses for all 11 exogenous compounds using respective optimized intensity cutoffs for tumor and stroma regions. Polycyclic aromatic hydrocarbons (blue), tobacco-specific nitrosamines (red), aromatic amines (green), organohalogen (gray).

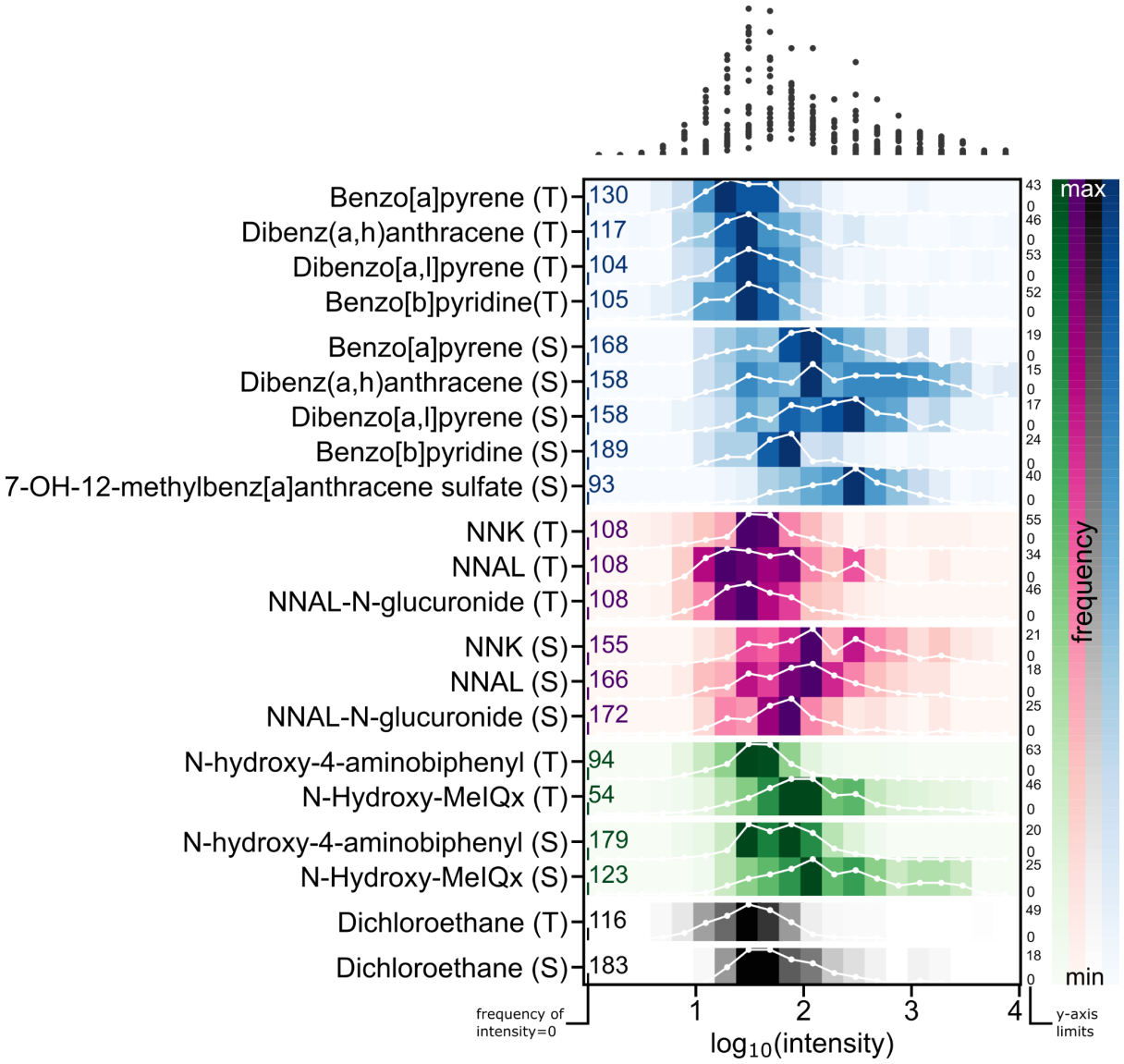

Supplemental Figure S9: Distribution of abundances for all measured exogenous compounds. Since the logarithmic values are visualized, missing values (intensity=0) are reported separately on the left. On the right, the y-axis limits are shown for each histogram row.

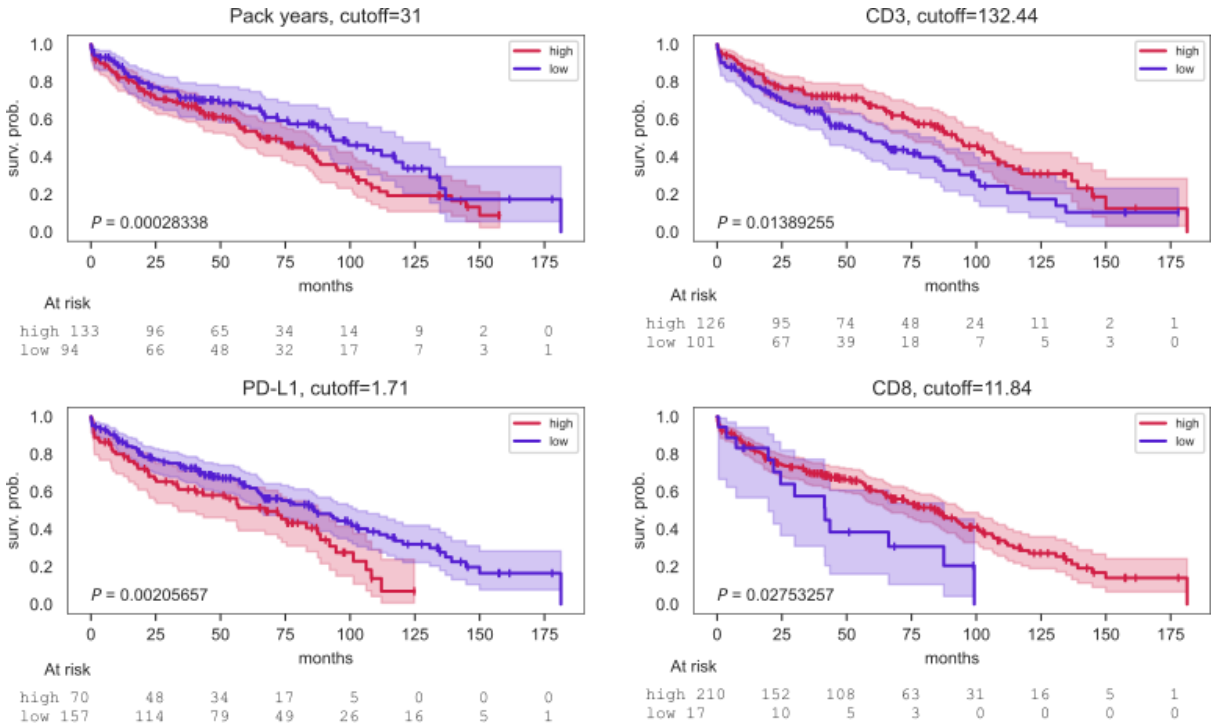

Supplemental Figure S10: Survival analysis for pack-years, tumor cell programmed death-ligand 1 (PD-L1) expression and CD3 and CD8 expression in tumor stroma. Optimal cutoffs were defined using the log-rank test.

RESULTS OF IDIOPATHIC PULMONARY FIBROSIS (IPF)

Carbon-bound exogenous compounds are also present in idiopathic pulmonary fibrosis.

In addition to lung cancer, other respiratory pathophysiological conditions, such as interstitial lung diseases, have been linked to environmental pollutants (1). We exploratively analyzed IPF tissues from ten patients and detected all exogenous compounds that were present in squamous-cell carcinoma (SQCC) tissues. Similar to SQCC, the highest abundance of carbon-bound exogenous compounds was found in and near the pigment regions. Exogenous compounds like benzo[b]pyridine, dibenz(a,h)anthracene, and dibenzo[a,l]pyrene are also enriched in regions with carbon deposits (Supplemental Figure S11). In comparison to normal lung parenchyma from healthy organ donors, a higher amount of anthracosis is present in IPF and a higher abundance of exogenous compounds was found ($P<0.05$, Supplemental Figure S12 - S14).

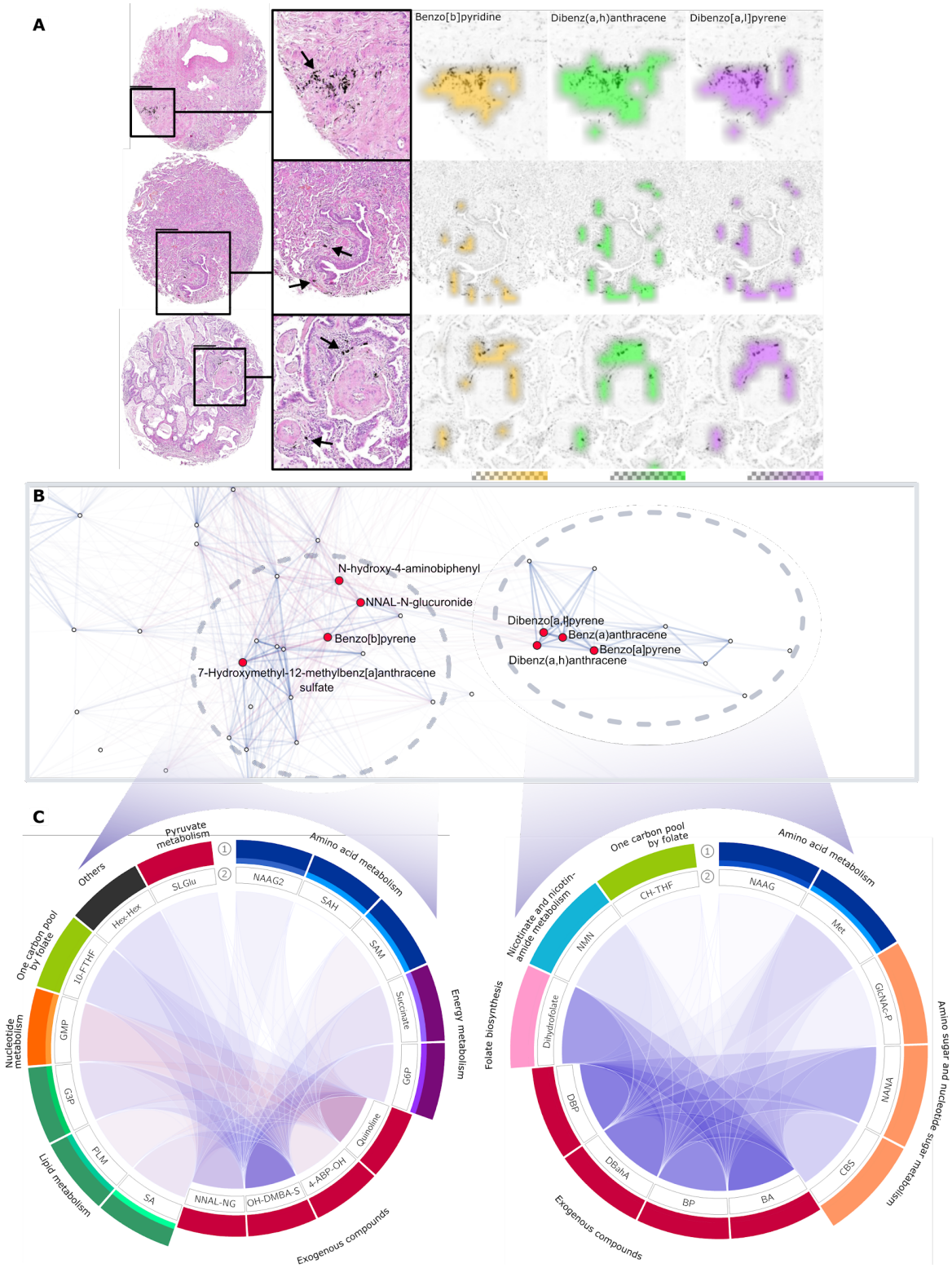

Supplemental Figure S11: Spatial correlation between carbon-bound exogenous compounds and endogenous metabolites in idiopathic pulmonary fibrosis (IPF). A: Histopathology of three IPF tissue cores containing carbon pigment (H&E staining) and ion maps of benzo[b]pyridine, dibenz(a,h)anthracene, and dibenzo[a,l]pyrene. Scale bar: 300 µm. **B**: Spatial correlation network of metabolites and carbon-bound compounds in IPF tissue. Nodes represent endogenous (white) and exogenous (red) compounds. Edges represent positive (blue) and negative (red) spatial correlations with the edge opacity increasing with the correlation coefficient. **C**: Circular plot of the two clusters

highlighted in B. Tracks: (1) pathway information; (2) compound abbreviation. Abbreviations: N-Acetylaspartylglutamylglutamate (NAAG2), S-adenosyl-L-homocysteine (SAH), S-adenosyl-L-methionine (SAM), glucose 6-phosphate (G6P), N-hydroxy-4-aminobiphenyl (4-ABP-OH), 7-OH-12-methylbenz[a]anthracene sulfate (OH-DMBA-S), NNAL-N-glucuronide (NNAL-NG), stearic acid (SA), palmitic acid (PLM), glycerol 3-phosphate (G3P), guanosine monophosphate (GMP), 10-formyltetrahydrofolate (10-FTHF), hexose-hexose (Hex-Hex), S-Lactoylglutathione (SL Glu), N-acetylaspartylglutamate (NAAG), methionine (Met), N-acetyl-D-glucosamine 6-phosphate (GlcNAc-P), N-acetylneuraminate (NANA), chitobiose (CBS), benz(a)anthracene (BA), benzo[a]pyrene (BP), dibenz(a,h)anthracene (DBahA), dibenzo[a,l]pyrene (DBP), nicotinamide D-ribonucleotide (NMN), 5,10-methenyltetrahydrofolate (CH-THF).

In IPF, spatial correlation networks show that both amino acid and lipid metabolism are affected by several carbon-bound compounds.

In contrast to the tumor and tumor stroma, spatial correlation networks for IPF tissues reveal two clusters of exogenous compounds and endogenous metabolites (Supplemental Figure S11B). The strongest correlation between exogenous compounds was found for dibenz(a,h)anthracene and dibenzo[a,l]pyrene (r_S=0.799). Another polycyclic aromatic hydrocarbon (PAH), benz(a)anthracene, also correlates with dibenzo[a,l]pyrene (r_S=0.714). In the second cluster, 7-OH-12-methylbenz[a]anthracene sulfate correlates strongly with D-glucose 6-phosphate (r_S=0.584). In SQCC, the strongest correlation of 7-OH-12-methylbenz[a]anthracene sulfate was with sn-glycerol 3-phosphate (r_S=-0.138), indicating that the compound has a much more pronounced metabolic effect in IPF tissues. Compared to the metabolites in tumor tissue, the metabolites correlating with exogenous compounds are associated with both amino acid metabolism and lipid metabolism (Supplemental Figure S11C). Other major pathway classes comprise energy metabolism and amino sugar and nucleotide sugar metabolism.

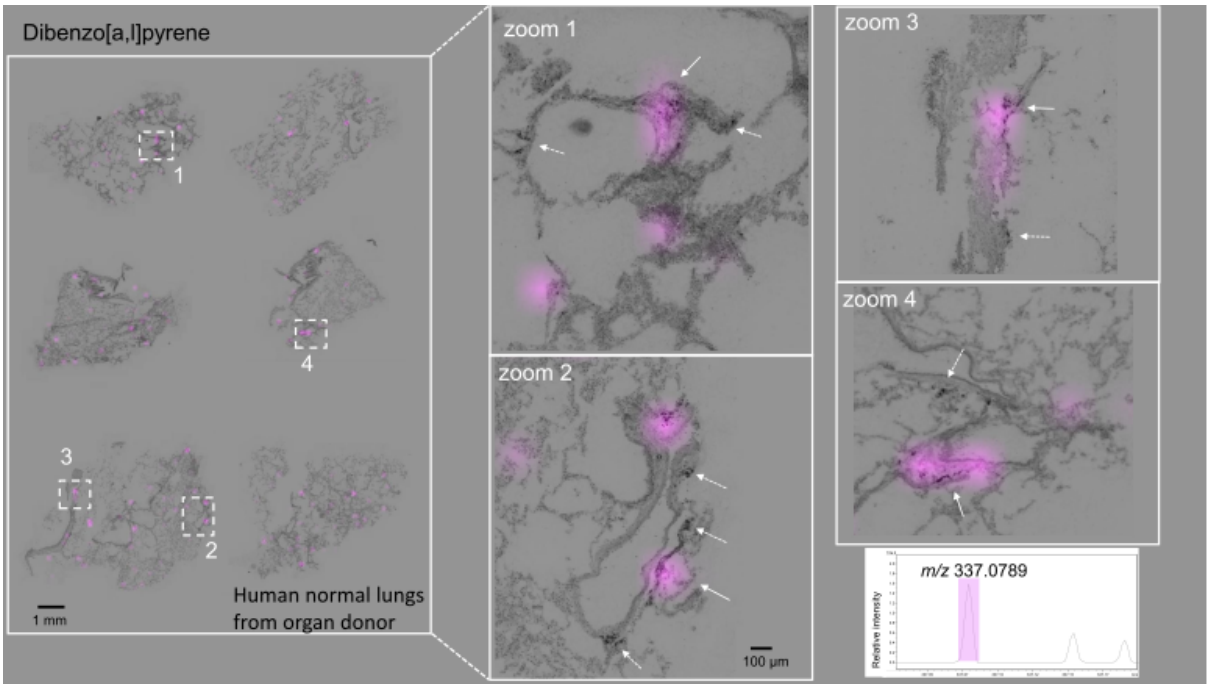

Supplemental Figure S12: Fresh frozen tissue sections from healthy organ donors. Normal lung tissues are shown after mass spectrometry imaging (MSI) *in situ* analysis. Dibenzo[a,l]pyrene (visualized in pink) is localized in and nearby carbon pigment. Note the heterogeneous distribution compared to the carbon pigment (white arrows). Mass spectrometry peak of *m/z* 337.0789 (highlighted in pink) for dibenzo[a,l]pyrene is shown on the lower right.

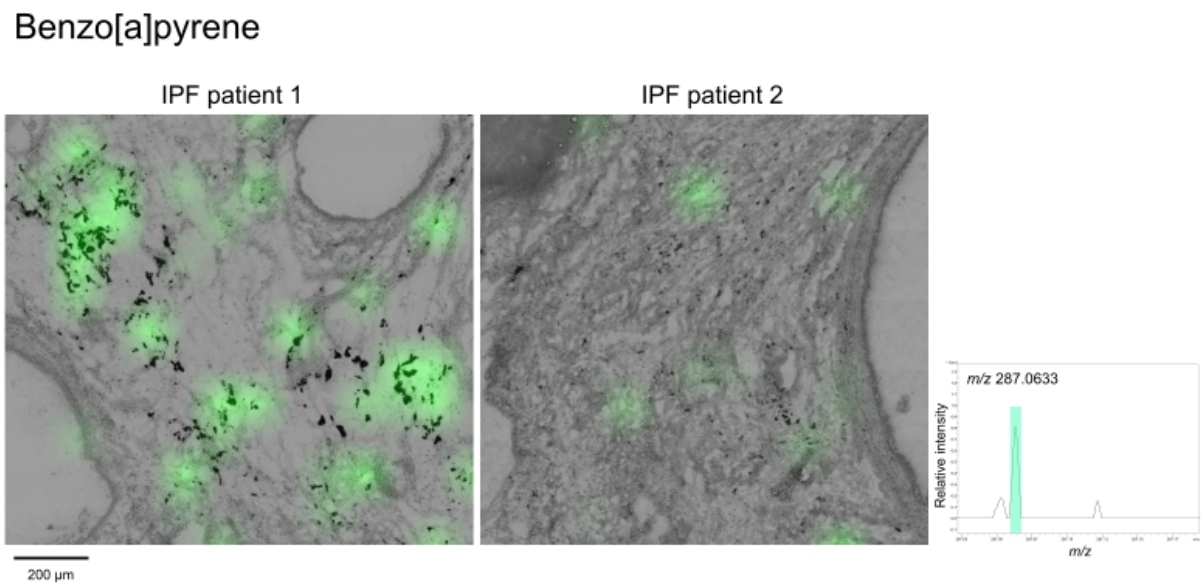

Supplemental Figure S13: Fresh frozen tissue sections from two patients with idiopathic lung fibrosis (IPF; tissue derived from explanted lungs). IPF tissues are shown after mass spectrometry imaging (MSI) *in situ* analysis. Benzo[a]pyrene (green) is localized in and nearby carbon pigment in patient 1, whereas patient 2 displays lower amounts of both pigment and benzo[a]pyrene. Mass spectrometry peak of *m/z* 287.0633 (highlighted in green) for benzo[a]pyrene is shown on the lower right.

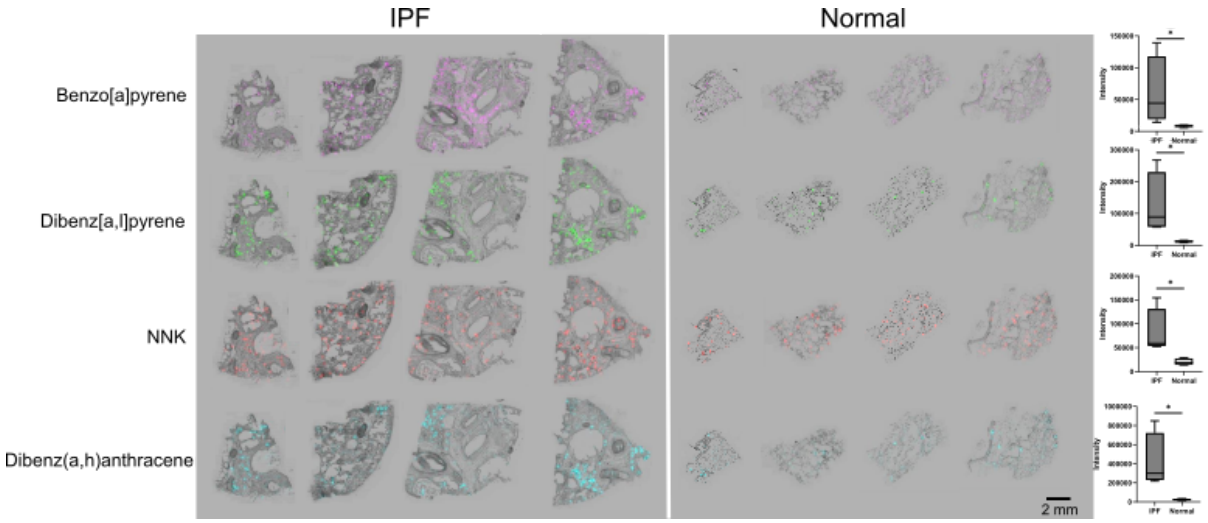

Supplemental Figure S14: Comparison of tissue sections from four patients with idiopathic lung fibrosis (IPF) and four normal lung tissues after mass spectrometry imaging (MSI) based *in situ* analysis. A higher abundance of benzo[a]pyrene (pink), dibenz[a,l]pyrene (green), 4-(methylnitrosamino)-1-(3-pyridyl)-1-butanone (NNK) (red), and dibenz(a,h)anthracene (blue) in IPF compared to normal lung parenchyma.

REFERENCES

1. Goobie GC, Nouraie M, Zhang Y, Kass DJ, Ryerson CJ, Carlsten C, et al. Air Pollution and Interstitial Lung Diseases: Defining Epigenomic Effects. Am J Respir Crit Care Med [Internet]. 2020; Available from: http://dx.doi.org/10.1164/rccm.202003-0836PP